Low-Degree Low-Order Solar P Modes As Seen By GOLF Onboard SoHO.

R.A. García[1] †, C. Régulo[2,3], S. Turck-Chièze[1], L. Bertello[4], A.G. Kosovichev[5], A.S. Brun[1,6], S. Couvidat[1], C.J. Henney[7], R.K. Ulrich[4] and F. Varadi[4,8]

[1] *Service d'Astrophysique, CEA/DSM/DAPNIA, CE Saclay, 91191 Gif sur Yvette, France*
[2] *Instituto de astrofísica de Canarias, 38205, La Laguna, Tenerife, Spain*
[3] *Dept. de Astrofísica Universidad de La Laguna, La Laguna, 38206, Tenerife, Spain*
[4] *Department of Physics & Astronomy, UCLA, Los Angeles, CA 90095-1562, USA*
[5] *HEPL, Stanford University, Stanford, CA 94305-4085, USA*
[6] *JILA, University of Colorado, Boulder, CO 80309-0440*
[7] *National Solar Observatory, 950 North Cherry Avenue, Tucson, AZ 85726-6732, USA*
[8] *Institute of Geophysics and Planetary Physics, UCLA, Los Angeles, CA 90095-1567*

Abstract. Data recovered from the GOLF experiment on-board the ESA/NASA SoHO spacecraft have been used to analyze the low-order low-degree solar velocity acoustic-mode spectrum below $\nu = 1.5$ mHz (i.e. $1 \leq n \leq 9$, $\ell \leq 2$). Various techniques (periodogram, RLAvCS, homomorphic-deconvolution and RLSCSA) have been used and compared to avoid possible bias due to a given analysis method. In this work, only the central frequencies of the solar acoustic resonances have been studied. 10 modes have been identified and their influence on the solar core is discussed.

Keywords: Sun: oscillations

1. Introduction

The detection of the low-degree low-order p modes is a very difficult task at frequencies below ~ 1.5 mHz. In this frequency range, the decrease of the mode amplitudes and the increase of the solar convective motions (solar background) reduce the signal to noise ratio of those modes complicating the search. Preliminary analysis of GOLF data by Régulo et al. (1998) provided a long list of possible identification of low-order acoustic modes. Additional lists based on the analysis of other data sets, both from space and earth-based networks, are also available (Anguera et al. 1992, Toutain et al. 1998, Fossat et al. 1999). Recently, Bertello et al. (2000b) detected three new p modes ℓ=0, n = 3, 5 and 6, by using a combination of data obtained from the GOLF and MDI instruments aboard SoHO and a new analysis technique called RLSCSA (Varadi et al. 1999, 2000).

† rgarcia@cea.fr

Low-degree low-order p modes are very important to understand the structure of the solar core. To illustrate this point, we plot in Figure 1 the following quantities:

-The observational error bars (vertical lines centered at zero) of the detected $\ell = 0$, 1 and 2 low-degree p modes. The larger error bars correspond to higher order acoustic modes which penetrate deeper into the solar interior.

- the difference between observational and theoretical frequencies extracted from a standard solar model. They are represented by crosses, diamonds and triangles respectively for the $\ell = 0$, 1 and 2 acoustic modes.

-the impact on the low degree frequencies of a 1 % and 0.5 % modification of the sound speed velocity in the solar core below 0.1 $R_\odot$ (dotted and dashed lines respectively).

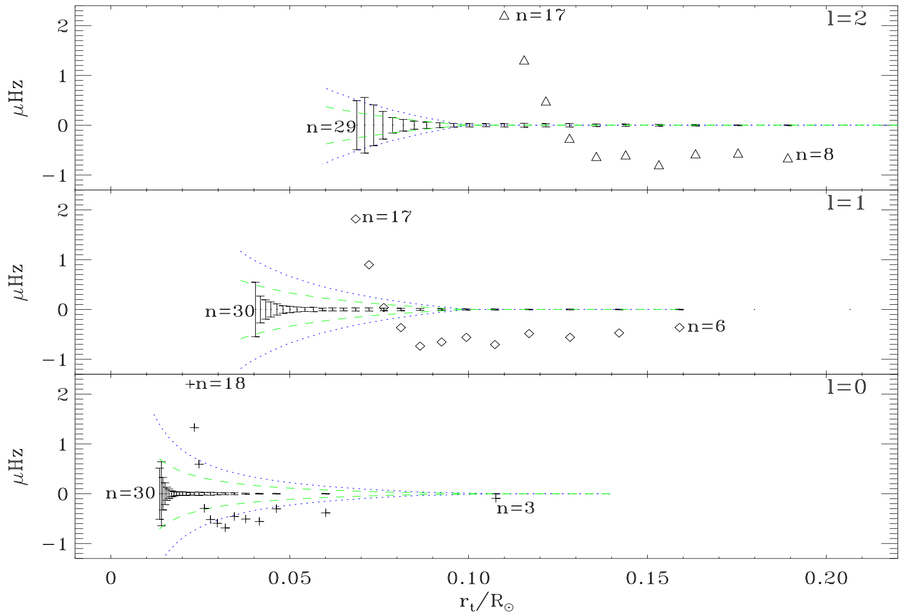

Figure 1. Comparison of the observational error bars (given in μHz) of the ℓ= 0, 1 and 2 p-mode frequencies (vertical lines centered in zero) with the difference, $\Delta\nu$, between their measured frequencies and the theoretical ones (crosses, diamonds and triangles) and with the frequency uncertainty due to a modification of 1 % (dotted lines) or 0.5 % (dashed lines) of the sound speed below 0.1 $R_\odot$, as a function of the fractional radius of their inner turning point $r_t = c_t L/\omega_{ln}$ where $L = \ell + 1/2$ (Lopés and Turck-Chiéze 1994). Each vertical tick-mark corresponds to 0.1 μHz. The order n of the first and last represented mode is written in the plot: 3 & 30 for ℓ=0, 6 & 30 for ℓ=1 and 8 & 29 for ℓ=2. The difference $\Delta\nu$ for the modes ℓ=0 n>18 and $\ell = 1$ and 2 n>17 are out of scale and are not shown in the plot.

The analysis of Figure 1 shows a large systematic deviation between the measured frequencies and those obtained from a standard solar model for the acoustic modes above $n \sim 16$. This is a well known effect, due to the complex physics of the outer layers (e.g. turbulence and magnetic fields) which are not taken into account in the standard solar models (see for example Figure 1 from Turck-Chièze et al. 1997). One can remove this frequency-dependent component by fitting a smooth function to the data. This function is usually deduced from modes of angular degree greater than three and applied to the data before they are used in any inversion technique, to prevent biases which may mask small effects coming from the core.

On the other hand, the low-order p modes ($n < 16$), which have external turning points deeper in the solar interior, are not sensitive to these problems and their determination is also more accurate (small error bars) since low-order p modes have longer lifetimes (narrower line widths). These modes have inner turning points above ~ 0.08 and ~ 0.12 $R_\odot$ for the ℓ=1 and 2 respectively. Thus, they are not able to distinguish any modification of the solar core below 0.1 $R_\odot$. However they would contribute to obtaining more information on the solar core as they have smaller error bars and they would help to increase the precision on the solar inversions. The radial modes with $3< n <16$ are particularly sensitive to the physics below 0.1 R$\odot$ (see Figure 1) and they are very useful to improve the study of the solar central region. They have small observational error bars permitting to distinguish changes of 0.5 % in the sound speed velocity below 0.1 $R_\odot$. Therefore, even though the internal turning points increase with decreasing order for a particular degree, the low-order acoustic modes will be the principal agents to extract the solar core information.

A description of the GOLF data along with a summary of the different techniques of analysis utilized in this paper are given in the next section. In section 3 we describe the results obtained from each indivual technique with particular emphasis on the detected acoustic mode. Section 4 contains a more general discussion of the results and a comprehensive table of low-degree low-order solar p modes. Finally, the implications for the solar interior structure of these new detected modes are discussed in the last section of the paper.

2. Data series. Creating the power spectrum estimates

In this work we use data from the GOLF instrument on-board the ESA/NASA SoHO spacecraft (Gabriel et al. 1995, 1997). GOLF measures the integrated line-of-sight velocity between the Sun and the spacecraft from two spectroscopic observations of the blue or red wing of the sodium doublet made every 10s (to reduce the amount of data, these measurements have been integrated to 20s or 80s for the present work). However, during the SoHO commissioning period, a problem in the rotating mechanism that allowed switching between the two wings of the sodium profile forced the GOLF instrument to work only in the blue wing. After the lost and recovery of the SoHO spacecraft in September 1998, GOLF has observed in the red wing.

The calibration procedure to extract the velocity from a single wing counting rates (recorded by two independent photomultipliers) is based on the methods described in Ulrich et al. (1999), Ulrich et al. (2000) and García et al. (in preparation). Thus, 1290 days of velocity residuals have been used in this study with a global duty cycle better than 88% from 1996 April 11 to 1999 October 22. Disregarding the SoHO lost period on summer 1998, the effective duty cycle of normal GOLF operations is better than 99%.

The solar p modes which we are interested in, are waves which are excited many times per second mainly by turbulent motions near the surface of the convection zone (Goldreich & Keeley 1977) and damped with time scales from several days to months at this frequency range (Libbrecht et al. 1986).

Thus, techniques other than the plain Fourier transform have been utilized to study this kind of problems (i.e. Régulo et al. 1998, Varadi et al. 1999). Techniques based on splitting the time series in different pieces are expected to help in reducing the incoherent sources of noise (as the solar velocity background for periods sufficiently long) and thus increase the signal to noise (S/N) ratio of the searched solar resonances. Also, in this frequency range the photon noise is only a factor of three below the measured solar velocity background, and its effect is not totally negligible. An additional problem comes from the fact that we are only observing for a finite period of time. Thus the final power spectrum is convolved with the window function corresponding to the time series length. This “windowing” introduces leakage from each frequency bin.

Six different techniques have been applied to reduce, as much as possible, one or more of the above effects increasing the S/N ratio of the searched p modes: periodogram (FFT) of the full— 1290 days —time series, periodogram of 3 independent chuncks of 400 days, Random-Lag Averaged Cross-Spectrum (RLAvCS), Homomorphic Deconvolution (HD) of the full series and an average of 5 series of 258 days, and Random-Lag Singular Cross-Spectrum analysis (RLSCSA). The use of different analysis techniques with the same data sets allows us to check the possible bias in the determination of the resonant frequencies of an individual one. In fact, the methods utilized here are very different and can be considered as independent. However, as we use the same data set, we also expect to have some correlation at the noise level.

2.1. Periodogram estimator of 1290 and 400 day series

Briefly, the periodogram estimator is the squared Fourier transform of the velocity time series. Two different lengths of the time series have been chosen. The first corresponds to the full 1290 days, and the second is 400 days.

This allows us to cut the full series in three independent chuncks avoiding 90 days of the SoHO lost period. The periodogram has been calibrated as the *one-sided power spectral density* (Press et al. 1994). We have artificially increased the frequency resolution by zero padding the time series a factor 4. These spectra show some candidate with a better S/N ratio.

2.2. RLAvCS

The Random-Lag averaged cross-spectrum estimator (RLAvCS) is a new method based on the properties of the average-cross spectrum, first introduced in helioseismology by Elsworth et al. (1995). The average cross-spectrum, CS, is defined as the average of the complex product of the Fourier transform of one data set, A, by the complex conjugate of the Fourier transform of another, B, i.e.,

$$CS(\nu) = \frac{1}{n}\sum_{i=1}^{n}(FFT(A(t_i)) \cdot FFT(B^*(t_i))) \quad , \tag{1}$$

where n is the total number of cross-spectra.

It has the main property of enhancing the coherent signals between the two data sets. This method has already been succesfully applied to the GOLF data to obtain the High Frequency Signals (HIPS) above the acoustic cut-off frequency by decreasing the photon noise of the measured channels (García et al. 1998). In the present case, this is not sufficient. We need to reduce the background noise, which is the same in the two channels, and not the photon noise. To do so, we need to make the cross spectrum between two data sets which are not simultaneous. In this case, the random background noise is not coherent. After averaging the cross spectra computed in this way, this background noise will be reduced. In practice, we need to cut the global series in many pieces of a given size (Nd) and then make the cross spectrum between all of them. These cuts can be done with a fixed lag, for example taking one subseries of Nd every $Nlag$ days. In this case, it can be demonstrated that the amplitude of those oscillations having a frequency which is multiple of $(a+0.5)/Nlag$, where a is an integer number, will be strongly reduced.

Another possibility is to use two sets of n random lags ($L1$ and $L2$) each one corresponding to one channel of the cross spectrum. These random lags give us the first point of the sub-series to be used in each iteration. It is a number between zero and $(np-Nd)$, where np is the total number of points of the global serie. We can express this method mathematically as follows:

$$RLAvCS(\nu) = \frac{1}{n}\sum_{i}^{n}(FFT(A(t(L1_i))) \cdot FFT(A^*(t(L2_i)))) \quad , \tag{2}$$

It is important to notice that while the background of the two substets of each iteration will always be incoherent, the acoustic modes will some-times be coherent because they are periodic and they are randomly re-excited. Therefore many average should be done to obtain a good signal to noise ratio of the periodic signals. In our case, two sets of n=35000 random lags have been used to obtain the initial point of each channel to make the cross spectrum. Each subseries has Nd=246 days long and has been zero padded to a total length of 1456.36 days which has a number of points close to 1290 days but being a power of 2 and 3 (to speed up the Fourier transform calculations).The selected parameters are a good trade-off between the frequency resolution and the number of sub-series to average and are based on our experience working with simulations and real data.

2.3. HD

The aim of the Homomorphic Deconvolution is to eliminate the non-stationary part of the signal which in the helioseismology case is the excitation functions of the modes (Baudin, Gabriel & Gibert 1993). The steps that the HD method follows are summarized hereafter.

$$FFT(s(t)) = S(\nu) \rightarrow \log(S(\nu)) \rightarrow FFT(\log(S(\nu))) = \text{Cepstrum} \rightarrow$$
$$\rightarrow \text{Filter.Cepstrum} = s_f \rightarrow FFT^{-1}(s_f) \rightarrow \exp[FFT^{-1}(s_f)] = S_f(\nu)$$

Briefly, for a given time series, $s(t)$, the HD method utilizes the Cepstrum, which is a complex transformation of the signal defined as

$$\text{Cepstrum} = FFT(\log(S(\nu))), \tag{3}$$

where $S(\nu) = FFT(s(t))$. The Cepstrum space (maplitude vs. quefrency) has the main property that the signal is concentrated at low quefrency while the excitation is mostly at high quefrencies. The simple solution is to cut the high part of the Cepstrum and to replace it by zeroes. Of course, the determination of the threshold could be a problem. Another way to filter the signal is to make an average of the Cepstrum of several time series. The filtered Cepstrum, s_f, is further processed to produce a final filtered spectrum, $S_f(\nu)$, defined as:

$$S_f(\nu) = \exp[FFT^{-1}(s_f)]. \tag{4}$$

For all the series the oscillating function will be the same but the noise will be different. The average will partially cancel the noise.

2.4. RLSCSA

The last method used in this paper is the Random-Lag Singular Cross-Spectrum analysis. It is based on the Singular Spectrum Analysis, developed for the first time in geophysics (e.g. Dettinger et al. 1995) to search for oscillations in short and noisy time series.

The RLSCSA method searches for oscillations in noise by the Singular Value Decomposition of cross-correlation matrices into a diagonal form where corresponding eigenvalues and eigenvectors can be identified. This new technique is described in details in two papers by Varadi et al (1999, 2000) and has been applied to data from SoHO, for the first time, by Bertello et al. (2000b). In short, the patterns of oscillations which are simultaneously present in two time series produce large eigenvalues in these cross-correlation matrices and their corresponding eigenvectors represent a filter on the original time series whose power spectrum contains the frequency structure of the oscillation. In general, one has to keep in the analysis only the eigenvalues, and the corresponding eigenvectors, which are above some threshold value. The actual patterns, their frequencies and relative phases, are measured by examining the spectral response of linear filters derived from these eigenvectors.

Since we are interested in modes with frequencies below $\sim$ 1.5 mHz, the 1290-day time series was sub-sampled to 300 seconds. The re-sampling has also the advantage to reduce the total number of points in the time series, which greatly benefits the application of RLSCSA. This task is accomplished by applying a low-pass filter to the original time series with a cutoff frequency at 1.66 mHz, which corresponds to the Nyquist frequency of the final sampling. The use of a filter before the sub-sampling is necessary in order to eliminate the signal distorsion due to aliasing from the large modes in the five minute band. For this purpose we use a linear-phase Finite Impulse Response digital filter specifically designed for this application. The filter design method is known as a Chebyshev approximation problem and has the important property that the weighted approximation error between the desired frequency response and the actual frequency response is spread evenly across the passband and the stop-band of the filter, minimizing the maximum error (Proakis & Manolakis 1996). After the re-sampling, a high-pass filter of the same type with a cutoff frequency at $\sim$0.1 mHz was applied to the time series in order to eliminate spectral leakage from the very low-frequency range. Before RLSCSA was applied, the time series was whitened using special filters which do not modify the phases of the signal (Bertello et al. 2000b). In order to be coherent between the different techniques, the background has been eliminated in all the methods.

3. Data analysis. Looking for the solar resonances

On the observational side, the critical points of our analysis are the criteria to search for these low amplitudes solar resonances. We have used the predicted frequencies as a good start up frequencies for those unknown modes, following the updated Saclay reference model (Brun, Turck-Chièze & Zahn

1999). The sensitivity of these predictions to some physical processes have been estimated by changing the values of the nuclear reaction rates and the opacities in their known uncertainties showing that these frequencies only change in less than ~ 1 μHz (see Figure 8 in Brun, Turck-Chièze and Morel (1998)) for any process modifiying the less known nuclear region of the Sun.

3.1. Periodogram estimator and ML analysis

A maximum Likelihood (ML) fitting code derived from that of Appourchaux et al. (1998) has been used as the noise power spectrum statistics is a χ^2 with two degrees of freedom. A symmetrical Lorentzian line profile is used to fit the observed spectra because the analysis is restricted to frequencies below $\nu \sim 1.5$ mHz. Thiery et al. (1999) showed that the small amplitudes and narrow line-widths of these modes do not permit a good determination of the asymmetric parameters. With this constraint, we could not apply a global fitting to the whole spectrum (i.e. Roca Cortés et al. 1998) and we have adopted a more common technique which consists in using a 10 μHz window centered on the theoretical predicted frequencies as said before. We have neglected the effects of higher degree modes ($\ell \geq 3$) which could slightly modify the resultant fitted parameters as their visibility with GOLF is very small. In all the multiplets we have fixed the relative amplitude ratio of the components and a common line-width for all the visible m components.

3.1.1. *Statistical considerations on the periodogram*

We need to know the confidence levels we can place in the acoustic mode candidates we find. That means we are looking for confidence levels we can apply on a periodogram. To perform this analysis, we compute the probability p_{det} for a single peak candidate with an amplitude S_{det} to be pure noise, as given by Appourchaux et al. (2000):

$$p_{det} = 1 - (1 - p)^N \tag{5}$$

where N is the number of peaks in the frequency bandwith we use to search for the candidate and p is the probability for one noise peak to exceed S_{det}. Actually, the confidence level we search is given by: $1 - p_{det}$. This level depends on both the noise statistical distribution on the power spectrum and the frequency bandwidth we use. The noise distribution on a periodogram is a basic exponential distribution (a scaled χ^2 with 2 degrees of freedom). Therefore, the probability p is given by:

$$p = \exp(-S_{det}) \tag{6}$$

Concerning the frequency bandwidth, we search for acoustic modes by intervals of 10 μHz. Thus, we can assign to each peak a p_{det} value. One minus this value is the confidence level of the single peak. Unfortunately, if we are only interested in peaks whose confidence level is better than 90%, we just find a few candidates. However, excepting the radial modes, the rest of the searched acoustic modes are not single peaks but multiplets. The probability to find noise peaks above a given threshold and separated a distance compatible with the components of a multiplet is extremely small. Thus, we consider multiplets instead of single peaks (Turck-Chièze et al. in preparation) to lower the detection thresholds while keeping a good confidence level. For these multiplets, we just retain the ones with a confidence level for the multiplet better than 90%.

The direct calculation of such levels turns out to be almost impossible, so we utilize Monte-Carlo simulations: we produce random noise data following an exponential distribution, and we search for the doublets and triplets contained in these data. The doublets are defined as: two peaks with an amplitude larger than a given threshold, and with a frequency separation standing in a given interval. Following the study of Provost, Berthomieu & Morel (2000), which supposes different core rotation laws, we have limited the splitting of two adjacent multiplet components to 0.2-0.6 μHz. It is meaningful to say that maybe not all the components of a given multiplet are expected to be excited at the same time. Assuming that the GOLF instrument only observes the $(l+m)$ even components, we can define the separation intervals we allow for the different types of multiplets (doublets $\ell = 1$ and 2 and triplets $\ell = 2$). For the triplets, we add another criterion, the symetry between the components: the difference of separation between the three components must be less than 0.15 μHz. With the Monte-Carlo simulations and the formula giving p_{det}, we are able to work out the probability for a single peak or a multiplet not to be pure noise. Actually, the whole statistical procedure leads to a small uncertainty when assigning a confidence level to a peak or a multiplet. This lack of accuracy is due to the limited number of realizations in the Monte-Carlo simulations and to the computation of the standard deviation in the interval where we search for candidates. We need the standard deviation value because the thresholds we compute are given in this unit.

3.1.2. *Application to the 1290 days series*

Table I sumarized the results obtained with the 1290 days velocity time series as explained in the previous section. The listed frequencies correspond to the central frequency of the fitted modes. The probability (written in brackets) is the confident level for a single peak (for the ℓ=0) and for the doublets (for the ℓ=1). No triplets ℓ=2 have been found. Thus, the mode ℓ=2 n= 9 has been detected as a doublet. One of the components was not excited above this threshold. For the ℓ=1, n=1 and 7, only one component of the multiplet has been detected. It has been fitted as a single lorentzian function and the 0.4

μHz error bar corresponds to the ambiguity of the detected component. The same problem arrives to the ℓ=2 n=8 and therefore an error bar of 0.8 has been taken.
As an indication the detection thresholds corresponding to a "better than 90% confidence level" are: 9.3 σ for the ℓ=0, 6.6 σ for the doublets $\ell = 1$, 7 σ for the doublets $\ell = 2$, and 5.5 σ for the triplets $\ell = 2$. These values are only valid for the periodogram based on 1290 day time series, when we look for candidates by intervals of 10 μHz.

Table I. Central frequencies of $\ell = 0$, 1 and 2 modes. The real (no zero padded) frequency resolution, $\Delta\nu$ is $\simeq$ 9 nHz. The values given in brackets are the confident levels. † Only one component of the ℓ=1 n=1 and 7 has been detected. The error of 0.4 μHz is given as a value of the uncertainty we have in the visible component. * Only one component of this ℓ=2 has been detected and an error bar of 0.8 μHz is given.

n	ℓ=0	ℓ=1	ℓ=2
1	-	284.666 $\pm$ 0.4 (90 %)†	-
2	-	-	-
3	-	-	-
4	-	-	-
5	-	-	-
6	972.612 $\pm$ 0.004 (80 %)	-	-
7	-	1185.983 $\pm$ 0.4 (95 %)†	-
8	1263.216 $\pm$ 0.006 (98 %)	1329.637 $\pm$ 0.007 (>90 %)	1394.613 $\pm$ 0.8 (60 %)*
9	1407.470 $\pm$ 0.012 (99 %)	1472.839 $\pm$ 0.008 (>90 %)	1535.860 $\pm$ 0.008 (>90 %)

3.1.3. *Application to 3 independent subseries of 400 days long*

To substantiate whether detected peaks in the observed full resolution power spectra are potentially signatures of real solar resonances, the 1290 day GOLF signal was divided into 3 independent sub-series of 400 days (excluding $\sim$90 days of the SoHO lost period). This segmentation of the time series was used to establish if the p-mode candidates exist in independent time series. However, we are dealing with signals that have very low signal-to-background ratios, therefore the above segmentation further reduces the visibility of these peaks, even if they are real. For this reason, only the $\ell = 0$ and 1 p modes have been considered and are listed in Table II.

The detection thresholds corresponding to a "better than 90% confidence level" with 10 μHz intervals for the 400 days time series have been reduced to: 8.1 σ for the ℓ=0 and 5.5 σ for the doublets $\ell = 1$.

As it is shown in this table, we are confident with the mode detection down to n=8 for the $\ell = 0$ and 1 for the three 400 day-segment analysis.

Table II. Central frequencies of ℓ = 0 and 1 modes given in μHz for 3 independent 400 days periods of time ($\Delta\nu \simeq 0.029\ \mu$Hz): ($a$) from 11/4/1996 to 16/5/1997; (b) form 17/5/1997 to 21/6/1998 and (c) from 18/9/1998 to 23/10/1999. The probability of each peak to be not due to pure noise is given in brackets. † Only one component of these modes have been detected. The error of 0.4 μHz is given as a value of the uncertainty we have in the visible component.

$\ell = 0$	400a	400b	400c
1	257.953 $\pm$ 0.011 (75 %)	-	-
2	-	-	-
3	-	-	-
4	-	-	-
5	-	-	-
6	972.648 $\pm$ 0.006 (93%)	-	-
7	-	-	1118.672 $\pm$ 0.006 (98%)
8	-	1263.213 $\pm$ 0.004 (99%)	1263.198 $\pm$0.083 ($\sim$ 100%)
9	-	-	1407.461 $\pm$0.005 ($\sim$ 100%)
$\ell = 1$	400a	400b	400c
1	-	-	-
2	-	-	-
3	-	-	-
4	745.747 $\pm$ 0.4 (89 %)†	-	-
5	-	-	-
6	-	-	-
7	-	1185.537 $\pm$ 0.020 (>90 %)	-
8	1329.679 $\pm$ 0.020 (>90 %)	1329.226 $\pm$ 0.4 (99 %)†	1329.216 $\pm$ 0.4 ($\sim$ 100%)†
9	1472.809 $\pm$ 0.011 (>90 %)	1472.853 $\pm$ 0.009 (>90 %)	1472.827 $\pm$ 0.006 (> 90 %)

Down to this order, each mode has been observed, at least one time, with more than 99 % of confidence level (values given in brackets) or in more than one 400 days time series. The listed acoustic modes with order $n < 8$, only appears in one of the subseries. They are potential p modes candidates but should be confirmed with the other analysis techniques that take into account all the available data.

Only one component of the acoustic mode ℓ=1 n=8 has been detected for the last two periods of time. As we did before, an error bar of 0.4 μHz has been taken as a measure of the ambiguity on the observed component of the multiplet. The confident levels given for the rest of the multiplets correspond to the probability of the doublet.

3.2. RLAvCS RESULTS

Table III summarized the results obtained with the RLAvCS applied to 1290 days of GOLF time series.

Table III. Central frequencies of ℓ =0, 1 and 2 modes. The frequency resolution, $\Delta\nu$ is $\simeq$ 8 nHz. The values given in brackets are the confident levels. † this ℓ=2 has been detected as a doublet and an error bar of 0.4 μHz is given.

n	ℓ=0	ℓ=1	ℓ=2
1	-	-	-
2	-	-	-
3	535.745 $\pm$ 0.003 (87 %)	-	-
4	-	-	-
5	-	-	-
6	-	-	-
7	-	1185.544 $\pm$ 0.003 (>90 %)	-
8	1263.216 $\pm$ 0.004 (>99 %)	1329.644 $\pm$ 0.008 (>90 %)	1394.605 $\pm$ 0.4 (70 %)†
9	1407.478 $\pm$ 0.013 (96 %)	1472.846 $\pm$ 0.006 (>90 %)	1535.880 $\pm$ 0.020 (>90 %)

The detection thresholds corresponding to a "better than 90% confidence level" with 10 μHz intervals are: 9.4 σ for the ℓ=0, 6.8 σ for the doublets $\ell = 1$, 7.2 σ for the doublets $\ell = 2$, and 5.6 σ for the triplets $\ell = 2$.

The mode ℓ=2, n=9 is detected as a triplet with a confident level >90%. In the other hand, the mode ℓ=2 n=8 has only been detected as a doublet and therefore an error bar of 0.4 μHz has been applied.

3.3. HD RESULTS

In this work, two different spectra have been used. The first one (5ceps.zeroes) was calculated by splitting the original time series into 5 independent pieces of $\sim$258 days ($\Delta\nu = 0.0406$ μHz) and for each one the Cepstrum was obtained. Before averaging, each Cepstrum was filtered by replacing the high part of the Cepstrum (1/4 of the points) with zeroes. Finally, the filtered Cepstra were averaged and the spectrum $S_f(\nu)$ was deduced.

For the other spectrum, no average was used. The total series of 1290 days was used ($\Delta\nu = 9$ nHz) and their Cepstrum obtained and filtered (cep.full). We have used two different filter methods, first replacing 2/3 of the Cepstrum by zeroes, and second, filtering 1/2 of the Cepstrum using a cosine shape for the cut. In most cases the results were compatible within 1-σ error bars and only in 4 cases (listed in brackets) one single method gives a candidate. The mode ℓ=1 n=7 is a special case. Each filter method has given a different component of the doublet. The central frequency has been computed as the average of both of them with an estimated error bar of 0.1 μHz.

It is important to notice that smaller independent data segments with 78 and 129 days were also considered but the results were similar and will not be shown.

Table IV. Central frequencies of ℓ =0,1 and 2 modes obtained by the HD method as described on the text.

$\ell = 0$	n	5ceps.zeroes	cep.full
	1	-	-
	2	402.85±0.06(*)	-
	3	-	535.76±0.01(*)
	4	-	-
	5	-	-
	6	973.06±0.06(*)	(973.03±0.01)
	7	1118.67±0.01	(1118.64±0.01)
	8	1263.21±0.01	1263.21±0.01
	9	1407.47±0.01	1407.465±0.01
$\ell = 1$	n	5ceps.zeroes	cep.full
	1	-	(284.67 ±0.40)
	2	-	-
	3	596.86±0.40	595.31±0.01
	4	747.93±0.23	-
	5	893.70±0.40	-
	6	1039.65±0.40	1039.30±0.08
	7	1185.57±0.03	1185.49±0.1
	8	1329.69±0.10	1329.645±0.02
	9	1472.83±0.01	1472.85±0.01
$\ell = 2$	n	5ceps.zeroes	cep.full
	1	384.34±0.80	385.76±0.80
	2	-	-
	3	663.56±0.80	663.52±0.80
	4	811.22±0.80	(811.20±0.80)
	5	957.80±0.80	957.79±0.80
	6	-	-
	7	1251.40±0.80	1251.40±0.80
	8	1394.81±0.10	1394.65±0.10

Around each theoretical p mode, a region of $\pm$ 10 μHz was selected. Unfortunately, there is no satisfactory significance test of the HD. Thus, all the peaks above 5 or 6 σ of the region (depending on the level of noise) are evaluated. Among these peaks, the ones within $\pm$ 2 μHz of the theoretical p mode frequency are selected. Usually only one peak appears in this interval. These peaks were fitted, when possible (using a standard non-linear least squares method), and are listed in Table IV for ℓ = 0, 1 and 2. The regions around a mode where more than one peak appear in the $\pm$ 2μHz interval are indicated in the Table with an asterisk.

In many cases for the ℓ = 1 and ℓ = 2 p modes it is not possible to fit the doublet or triplet because only one of the m components is evident. For these modes it is assumed that the error is $\pm$ 0.40 μHz for ℓ = 1 and $\pm$ 0.80 μHz for ℓ = 2, because of the ambiguity on which component has been observed.

3.4. RLSCSA RESULTS

Once a spectrum is obtained from the RLSCSA and a mode has been positively identified, standard symmetrical procedures to fit the line profile of this mode can be used. In the frequency range below $\sim$ 1.5 mHz we have been able to identify nine low-degree ($\ell < 3$) low-order ($n < 10$) p modes. The frequencies of these modes, as obtained from the fit, are listed in Table V.

Table V. Central frequencies of ℓ =0,1 and 2 modes obtained by the RLSCSA method using 1290 days of the GOLF experiment as described on the text.

n	ℓ=0	ℓ=1	ℓ=2
1	-	-	-
2	-	-	-
3	535.729 $\pm$ 0.009 (41)	-	-
4	-	-	-
5	-	-	-
6	972.609 $\pm$ 0.003 (111)	-	-
7	-	1185.549 $\pm$ 0.003 (11)	-
8	1263.215 $\pm$ 0.002 (5)	1329.662 $\pm$ 0.010 (1)	1394.671 $\pm$ 0.003 (17)
9	1407.479 $\pm$ 0.003 (9)	1472.857 $\pm$ 0.003 (4)	1535.865 $\pm$ 0.004 (8)

The corresponding statistical 1 σ errors were obtained from the inverse of the Hessian matrix associated with each fit (e.g. Anderson et al. 1990). The relatively small error (compared to a nominal frequency resolution of 1/1290 days $\sim$ 9 nHz) associated to most of the modes in the table is the result of a combination of different factors: The length of the time series used in the analysis, the very narrow nature of these modes, and the fact that RLSCSA greatly increases their signal to background ratio. However, it is important to point out that the formal fitting uncertainty may be slightly different from the actual frequency precision, which is presently unknown.

At the present time some work has been done to introduce confident levels in the RLSCSA but the results are not yet fully tested. However, a power-based rank test has been applied to the spectrum. To do so, the spectrum between 500 and 1600 μHz has been re-sampled to 2200 bins of 0.5 μHz width each. The obtained ranking for each mode is listed in brackets beside each frequency in Table V. Except for the mode ℓ=0, n=6, all the rest is within the 40 highest peaks of the spectrum and 7 of the candidates are placed among the first 11 peaks. This result shows how prominent are the candidate modes and how powerful this method is. Moreover, all modes listed in Table V correspond to peaks in the power spectrum which are the most prominent signature in a frequency range $\pm$ 5 μHz around the predicted frequency of the mode.

4. Discussion

Six independent methods have been applied to the same GOLF velocity time series in order to explore the low frequency p-mode band of the power spectrum and study possible bias from a given analysis method. In Figure 2 the spectral regions corresponding to the modes ℓ=0 n=3 and ℓ=1 n=7 are shown for three of the analysis.

From the analysis of the 3 independent subseries of 400 days we have learned that at low frequency, the stability with time of the low-degree acoustic modes is very weak. For example, the mode ℓ=0 n=7 can be seen with 98 % confident level in the last 400 days period, while in the other two periods there is nothing statistically significant. This is a very important result because one could think that these modes should be stably present in the spectrum due to their long lifetimes. However, the coherence of these modes could be destroyed before their characteristic decay time either by the excitation mechanism (if it is out of phase) or by interferences with the convective noise.

Concerning the relative amplitude of the peaks within a multiplet, we have verified that only one component of the multiplet can be excited during very long periods of time (more than 2 years). To illustrate that, the mode ℓ=1 $n = 8$ is a very good example. Only the component $m = -1$ is visible in the last two considered periods of 400 days with an amplitude around 20 σ while there is no trace of the $m = 1$.

The other five methods use the whole data series to produce a single final spectrum that can be analyzed and fitted. All the rest of the discussion will be based on these five methods.

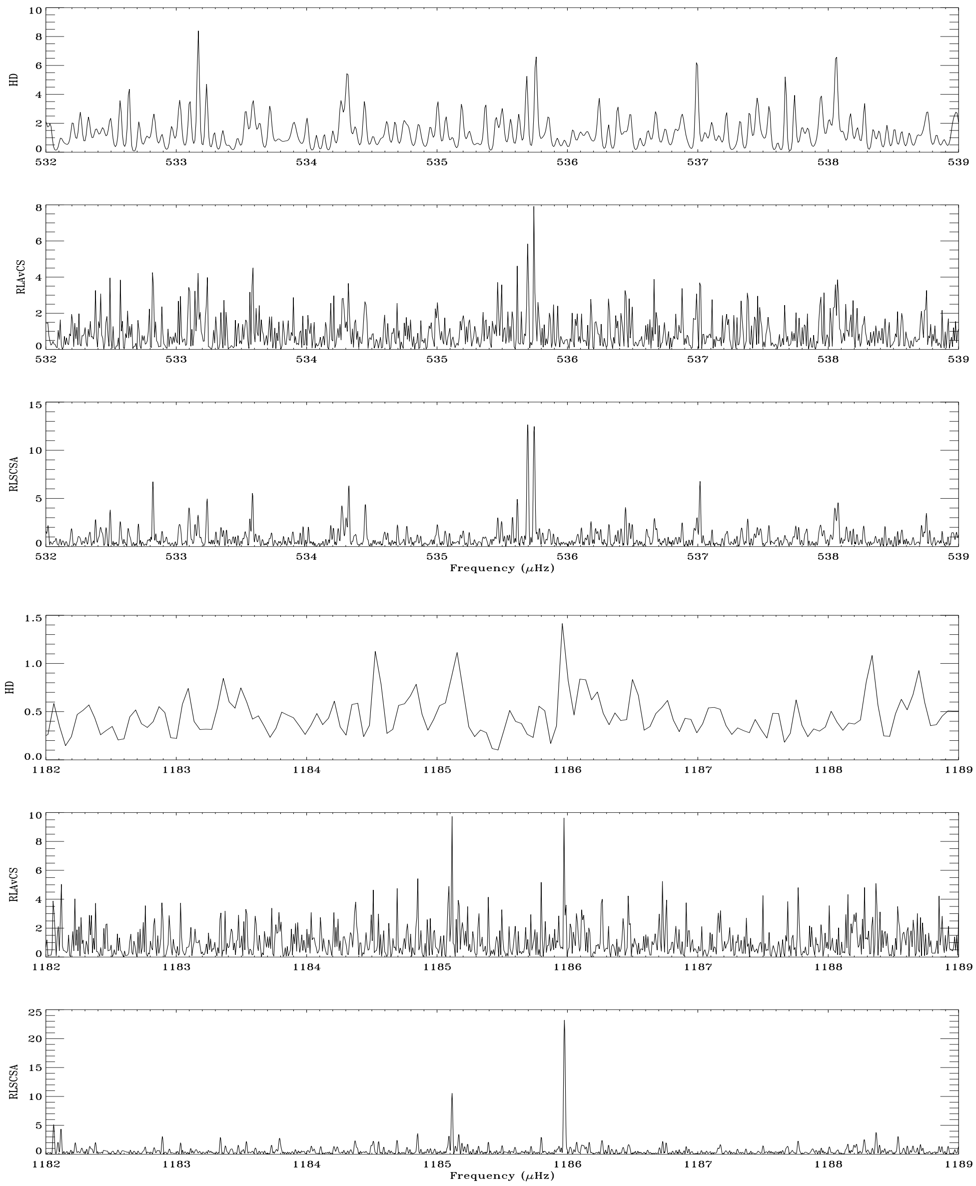

Figure 2. Spectral region corresponding to the modes ℓ=0 n=3 at 535.74 μHz and ℓ=1 n=7 at 1185.54 μHz computed with three of the analysis used in the paper. The HD figures correspond to cep.full and 5ceps.zeroes for the ℓ=0 and 1 respectively.

Comparing the frequencies given by each analysis technique one against another we obtain that from 6 out of 10 possible comparison of two methods, 80 % of the modes have the same frequency in the two compared analysis within 1 standard deviation; 8 out of 10 have 70 %; 9 out of 10 have 65 % and all the analysis have 55% of common frequencies within this range. No systematics effects in the frequencies have been found. However, the error bars of the two HD spectra are bigger (a factor $\sim$ 3) while the RLSCSA usually are among the smallest in comparison with the other methods.

Encouraged by these results we have built an average table of frequencies (Table VI). To avoid give any privilege to a particular analysis and to take into account the accuracy of each technique we have done a weighted average of all the frequencies. We have also decided not to use the detected components of a multiplet where only one have been measured. It is important to notice that this table is just a tool that show as a set of frequencies which are independent on the analysis technique that has been used. In the next section, we will invert this set of frequencies to infer information on the solar structure.

To include a frequency in the table it should appear, at least, in three or more of the analysis. However, the mode ℓ=0 n=7 is listed as a candidate (in brackets) as it only appears in two of them.

To compute an estimation of the error we have used three different approaches. The first one (column labeled *error 1* in table VI) is a weighted average of the individual errors. It generates small error bars, typically less than 5 nHz, which is an under-estimation of the real uncertainty we have between all the analyses. The second one (*error 2*) is the standard deviation of the central frequencies. In this case, 75% of the frequencies obtained with the different methods lie within 1 σ, while 100% lie within 2 σ. The mode ℓ=0 n=6 has a standard deviation which is nearly an order of magnitude bigger than the others. Looking carefully there are two methods (periodogram and RLSCSA) giving a central frequency of $\sim$ 972.6 μHz with error bars smaller than 6 nHz while the two HD gives a central value around 973.0 with error bars a factor of 10 higher. These last two frequencies could not correspond to a good detection of this mode. Removing these two frequencies from the calculation we obtain a candidate frequency (as seen only by two methods) at 972.610 μHz (listed in brackets in table VI) with an error bar of 2 nHz. The *error*2 is systematically bigger than *error*1. Even though, our *error*2 is, in the worst case, more than a factor of 2 better than the error bars of the frequencies of the modes above ν=1.5 mHz.

Comparing our results with the low-degree low-order p-mode identifications done by Bertello et al. (2000b) for a joint GOLF-MDI analysis of 759 days velocity time series, there are 9 common identifications. Using *error*1 two of the modes, the ℓ=1 n=7 and the ℓ=2 n=8 are respectively within 2- and

Table VI. Central averaged weighted frequencies calculated as explained on the text.

$\ell = 0$	ν	error 1	error 2
1	-	-	-
2	-	-	-
3	535.745	0.004	0.016
4	-	-	-
5	-	-	-
6	972.634	0.004	0.321
	(972.610)	(0.003)	(0.002)†
7	(1118.655)	(0.010)	(0.021)
8	1263.215	0.003	0.004
9	1407.477	0.005	0.008
$\ell = 1$	ν	error 1	error 2
1	-	-	-
2	-	-	-
3	-	-	-
4	-	-	-
5	-	-	-
6	-	-	-
7	1185.547	0.003	0.035
8	1329.645	0.009	0.024
9	1472.852	0.005	0.013
$\ell = 2$	ν	error 1	error 2
1	-	-	-
2	-	-	-
3	-	-	-
4	-	-	-
5	-	-	-
6	-	-	-
7	-	-	-
8	1394.671	0.003	0.099
9	1535.864	0.005	0.011

3-σ respectively while the rest are within 1-σ error bars. Taking into account *error*2 all of them are within 1-σ error bars.

5. Inversion results

Figure 3 illustrates the difference between the square of the sound speed extracted from the Sun and the one coming from two solar models (Christensen-Dalsgaard et al. (1996) and Brun, Turck-Chièze and Zahn (1999)). The differences between the two models are clearly identified. The second model includes the pre-main sequence and an update of the reaction rates, of the age and of the opacity coefficients (see discussion of the comparison of different models in Turck-Chièze et al. 1998).

In this analysis, we consider the frequencies proposed in table VI with the *error 2* coupled to the ones by Bertello et al. (2000a) for GOLF data ℓ=0,1,2 ν> 1.5 mHz and the frequencies of ℓ =3-300 obtained by Rhodes et al. (1997). An optimally localized averaging inversion method developed by Gough & Kosovichev (1988) and Kosovichev (1999) is used to determine the hydrostatic structure of the Sun.

First we compare the results of the upper figures with the results obtained by Bertello et al. (2000b) who show the same kind of inversion except that the low frequencies are extracted from a combined analysis of GOLF and MDI. The general profile is very similar in the core. The slight differences are attributed to the presence of two more low-order p modes in Bertello et al. (2000b) and the smaller error bars. It is now clearly established that small differences in the frequencies of the low degree low order p modes have a large impact on the inversion of the whole radiative zone when the error bars are very small. This may produce artificial (or real) bumps along the solar profile.

As we mentioned in the introduction, the interest of low order acoustic modes is that their outer turning points are less sensitive to the turbulent outer layers. Consequently, their corresponding frequencies are less sensitive to any bias in the inversion procedure which could be caused by surface effects or time variations of the outer layers during the solar cycle. This may lead to spurious effects when the information on the solar core, extracted from low degree modes obtained from long time series, is coupled with higher degree modes, extracted from a different instrument and a different period of time.

To see the influence of such problem we show in the lower part of Figure 3 two inversions using only modes of orders n < 16 for l=0, 1 and 2. It leads to a modification of the sound speed profile below 0.1 $R_{\odot}$, as expected. We note that the difference is at most 0.1%. We can therefore be confident in the global procedure and the general coherence of the analysis. However, the

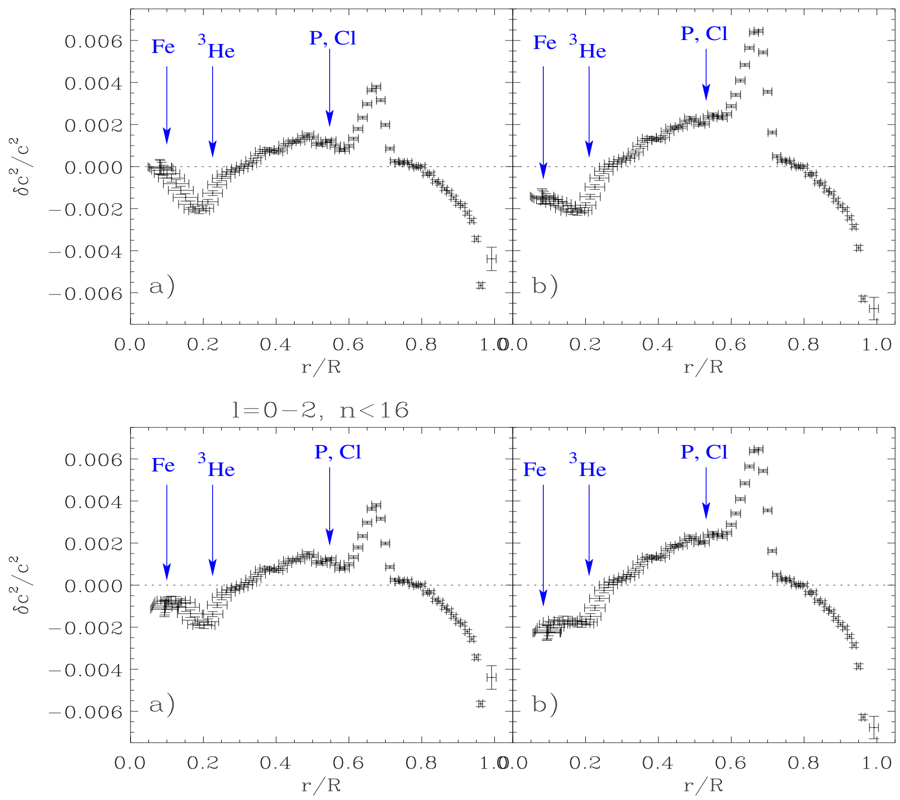

Figure 3. Relative difference between the sound speed squared in the Sun and the corresponding sound speed of two different solar models, model S of Christensen-Dalsgaard et al. (1996) ((a) panels) and Saclay model by Brun, Turck-Chiéze and Zahn (1999) ((b) panels). The top panels show the inversion using all the modes listed in Table VI, with the modes of Bertello et al. (1999a) for ℓ= 0-2 (ν > 1.5 mHz) and the modes ℓ=3-300 from Rhodes et al (1997). The bottom ones show the same inversion after removing the p-mode frequencies of ℓ =0-2 above n > 16. The arrows show the regions where specified species (Fe, ^{3}He, P, Cl) contribute significantly to the opacity.

spatial resolution of this inversion is slightly reduced by the absence of high order modes.

In Figure 3, several bumps are present in the difference of the squared sound speed for both models. This may be due to an effect of opacities caused by an incorrect determination of the elemental composition along the solar radius in the adopted models, or by a small error in the calculation of the opacity coefficients. In fact, a well known effect is discussed by Iglesias and Rogers (1996) concerning the quality of the equation of state and the introduction of P, Cl, K, Ti, Cr and Mn in the opacity coefficients. The absence of these elements in the opacity coefficients used in the first model ((a) panels) is at the origin of the dip around 0.6 $R_{\odot}$. The other bumps may be attributed to different elements as discussed in Turck-Chièze (1998) which may involve Si, ^{3}He and ^{56}Fe. We have indicated by arrows the location where selected elements (e.g. Fe, ^{3}He, P, Cl) influence significantly the opacity coefficients through bound-bound processes and, consequently, the sound speed. The actual sensitivity of the opacity to a particular species depends on its relative abundance in the solar composition. The amplitude of the bumps is of the order of 0.1 or 0.2 % which corresponds to a variation of 1 or 2 % of the opacity coefficients. This variation can be translated to a $\sim$ 10 % uncertainty on the abundances of specific species in the radiative region.

The central part of the Sun is still slightly dependent on the low frequency modes used in the inversion but is much better established than before because of the newly observed radial modes. The fact that there is no clear deviation from the classical solar model excludes strong mixing in the core. The accuracy reached nowadays allows a check of the sensitivity to the nuclear processes. These different points are discussed in Turck-Chièze et al. (2000). An effect coming from the early stage of solar evolution (Bertello et al. 2000b) or a change in the assumed iron abundances in the very central part of the Sun cannot be excluded at this time.

6. Conclusion

This paper shows the interest of using low-degree low-order p modes to determine the structure of the solar core. After nearly four years of measurements on-board the SoHO spacecraft, the GOLF experiment, due to its high instrumental stability, is able to detect 10 modes below $\sim$ 1.5 mHz, using three different analysis method. This is particularly useful as the central frequencies of these acoustic modes are accurately determined ($\sim$ 10 nHz, $\Delta\nu/\nu \sim 10^{-5}$). They are also less sensitive to surface effect variations caused by the solar activity. This allows as to deduce detailed information on the solar core which puts more severe constraints on the physical processes.

A better spatial resolution on the inversions would help to diagnose the sources of the present discrepancies found in the solar core. This will be achieved when all the low frequency acoustic modes will be detected and by progressing on g mode detection which can only be done by integrating longer time series.

We can be confident that during the extended SoHO mission we will be able to obtain all the p modes down to n=1.

Acknowledgements

The GOLF experiment is based upon a consortium of institutes (IAS, CEA/Saclay, Nice and Bordeaux Observatories from France, and IAC from Spain) involving a large number of scientists and engineers, as enumerated in Gabriel et al. (1995). SoHO is a mission of international cooperation between ESA and NASA. The authors want to thank J. Charra and C. Renaud for their daily work surveying the GOLF instrument, Jérôme Ballot for his work on the solar core and S. Turcotte for useful scientific discussions.

References

Anderson E.R., Duvall Jr T.L. & Jefferies S.M. 1990, Ap. J., 364, 699

Anguera Gubau M., Pallé P.L., Pérez Hernandez F., Régulo C. & Roca Cortés T. 1992, A&A 255, 363

Appourchaux T., Gizon L. & Rabello-Soares M.C. 1998, A&A, 132, 107

Basu, S., Turck-Chièze, S., Berthomieu, Brun, A. S., Corbard, T., Gonczi, G., Christensen-Dalsgaard, J., Provost, J., Thiery, S., Gabriel, A. H., Boumier, P., 2000, Ap. J., 535, 1078B

Baudin F., Gabriel A.H. & Gibert D. 1993, A & A, 276, L1

Bertello L., Henney C.J., Ulrich R.K., Kosovichev A.G., Roca Cortés T., Thiery S., Boumier P. & Turck-Chèze S. 2000a, Ap. J., 535, 1066

Bertello L., Varadi F, Ulrich R.K., Heenney C.J., Kosovichev A.G. García R.A. & Turck-Chièze S. 2000b, Ap. J., 537, L143

Brun A.S., Turck-Chièze S. & Morel P. 1998, Ap. J. 506, 913

Brun A.S., Turck-Chièze S. & Zahn J.P. 1999, Ap. J., 525, 1032

Christensen-Dalsgaard J., Däppen W., Ajukov S.V., Anderson E.R., Antia H.M., Basu S., Baturin V.A., Berthomieu G., Chaboyer B., Chitre S.M., Cox A.N., Demarque P., Donatowicz J., Dziembowski W.A., Gabriel M., Gough D.O., Guenther D.B., Guzik J.A., Harvey J.W., Hill F., Houdek G., Iglesias C.A., Kosovichev A.G., Leibacher J.W., Morel P., Proffitt C.R., Provost J., Reiter J., Rhodes E.J.Jr, Rogers F.J., Roxburgh I.W., Thompson M.J. & Ulrich R.K. 1996, Science, 272, 1286

Dettinger M.D., Ghil M., Strong et al. 1995, *EOS*, Trans. AGU, 76, 12

Elsworth Y.P., Howe R., Isaak G.R., McLeod C.P., Miller B.A., New R. & Wheeler S.J. 1995, A & AS, 113, 379.

Fossat E., Kholikov Sh., Gelly B., Schmider F.X., Fierry-Fraillon D., Grec G., Pallé P.L., Cacciani A., Ehgamberdiev S., Hoeksema J.T. & Lazrek M. 1999, A & A, 343, 608

Gabriel A.H., Grec G., Charra J., Robillot J.M., Roca Cortés T., Turck-Chièze S., Bocchia R., Boumier P., Cantin M., Céspedes E., Cougrand B., Cretolle J., Dame L., Decaudin M., Delache P., Denis N., Duc R., Dzitko H., Fossat E., Fourmond J.J., García R.A., Gough D., Grivel C., Herreros J.M., Lagardere H., Moalic J.P., Pallé P.L., Petrou N., Sánchez M., Ulrich R.K., & van der Raay H.B. 1995, Sol. Phys., 162, 61

Gabriel A.H., Charra J., Grec G., Robillot J.M., Roca Cortés T., Turck-Chièze S., Ulrich R.K., Basu S., Baudin F., Bertello L., Boumier P., Charra M., Christensen-Dalsgaard J., Decaudin M., Dzitko H., Foglizzo T., Fossat E., García R.A., Herreros J.M., Lazrek M., Pallé P.L., Petrou N., Renaud C. & Régulo C. 1997, Sol. Phys., 175, 207.

García R.A., Pallé P.L., Turck-Chièze S. et al. 1998, Ap. J., 504, L51

Goldreich P. & Keeley D.A. 1977, Ap. J. 211, 934

Gough, D.O., & Kosovichev, A.G. 1988, in Seismology of the Sun and Sun-like stars, ed. E. J. Rolfe (Paris: ESA), 195.

Kosovichev, A.G. 1999, J. Comp. Appl. Math., 109, 1

Harvey J.W. 1985 in “Probing the depths of a Star: the study of solar oscillations from space”, R.W. Noyes and Rhodes E.J.Jr. (eds.), JPL 400-327, 1985

Nigam R. & Kosovichev A.G. 1998, Ap. J., 505, L51

Libbrecht K.G., Popp B.D., Kaufman J.M. & Penn M.J. 1986, Nature 323, 235

Lopès, I.P. & Turck-Chièze, S., 1994, Astron. Astrophys. 290, 845

Pallé P.L., Fossat, E., Régulo, C., Loudagh S., Schmider F.X., Ehgamberdiev S., Gelly B., Grec G., Khalikov S. & Lazrek M. 1993, A&A 280, 324

Multitaper and Conventional Univariate Techniques, Cambridge University Press

Press W.H., Teukolsky S.A., Vetterling W.T. & Flannery B.P. 1994, Numerical Recipies in Fortran: the art of scientific computing 2nd ed., Cambridge University Press

Proakis J.G. and Manolakis D.G. 1996, Digital Signal Processing (Prentice-Hall Inc.: Upper Saddle River, NJ)

Provost J., Berthomieu G., & Morel P. 2000, A&A, 353, 775

Régulo C., Varadi F., García R. A., Roca Cortés T., Ulrich R.K., Gabriel A.H., Grec G., Robillot J.M. & Turck-Chièze 1998 in: S. Korzernnik and A. Wilson (eds.), Proc. SoHO 6/GONG 98 Workshop ESA SP-418, ESA Publications Division, Noordwijk, NL, 305

Rhodes E.J. Jr, Kosovichev A.G., Schou J., Scherrer P.H., Reiter J., 1997, Sol. Phys., 175, 287

Roca Cortés T., Lazrek M., Bertello L., Thiery S., Baudin F., Boumier P., Gavryusev V., García R.A., Régulo C., Ulrich R.K., Grec G., Robillot J.M. & Turck-Chièze S. 1998 in: S. Korzernnik and A. Wilson (eds.), Proc. SoHO 6/GONG 98 Workshop ESA SP-418, ESA Publications Division, Noordwijk, NL, 329

Thiery S., Boumier P., Gabriel A.H., Bertello L., Lazrek M., García R.A., Grec G., Robillot J.M., Roca Cortés T., Turck-Chièze S., Ulrich R.K. 2000, A&A, 355, 743

Toutain T., Appourchaux T., Fröhlich C., Kosovichev A.G., Nigam R. & Scherrer P.H. 1998, Ap. J. 506, L147

Turck-Chièze S., Basu S., Brun A.S. Christensen-Dalsgaard J., Eff-Darwich A., Lópes I., Hernández Perez F., Berthomieu G., Provost J., Ulrich R.K., Baudin F., Boumier P., Charra J., Gabriel A.H., García R.A., Grec G., Renaud C., Robillot J.M. & Roca Cortés T. 1997, Sol. Phys., 175, 247

Turck-Chièze, S. 1998, in Solar composition and its evolution - from core to corona, ed. C. Fröhlich, M.C.E. Huber, S. K. Solanki, R. Von Steiger, p 125.

Turck-Chièze S., Basu S., Berthomieu G., et al. 1998, in Proc. of the SOHO6/GONG 98 Workshop on Structure and Dynamics of the interior of the Sun and Sun-like stars, ed. Korzennik S.G. & Wilson A., ESA SP-418, vol 1, 555

Turck-Chièze S., García R.A., Couvidat S., et al. 2000, Ap. J., in preparation

Turck-Chièze S., Nghiem P., Couvidat, S. & Turcotte, S., 2000, Sol. Phys., this volume

Ulrich R.K., García R.A., Robillot J.M., Boumier P., Bertello L., Turck-Chièze S., Charra J., Gabriel A., Grec G. & Roca Cortés T. 1998 in: S. Korzernnik and A. Wilson (eds.), Proc. SoHO 6/GONG 98 Workshop ESA SP-418, ESA Publications Division, Noordwijk, NL, 353

Varadi F., Pap J.M., Ulrich R.K., Bertello L., Henney C.J. 1999, Ap. J., 526, 1052

Varadi F., Ulrich R.K., Bertello L. & Henney C.J. 2000, Ap. J., 528, L53